Biochemical and Biophysical Research Communications 526 (2020) 880–888

Contents lists available at ScienceDirect

Biochemical and Biophysical Research Communications

journal homepage: www.elsevier.com/locate/ybbrc

# Loss of heterozygosity for Kras$^{G12D}$ promotes REDD1-dependent, non-canonical glutamine metabolism in pancreatic ductal adenocarcinoma

Yu Ma [a], Yuan Li [a], Sunkai Ling [a], Xiaoxue Li [a], Bo Kong [b], Mingyue Hu [a, c, **], Peilin Huang [a, *]

[a] School of Medicine, Southeast University, Nanjing, 210009, China
[b] Department of Surgery, Klinikumrechts der Isar, School of Medicine, Technical University of Munich (TUM), Munich, 81675, Germany
[c] Department of Gastroenterology, Southeast University, Dingjiaqiao 87, Gulou District, Nanjing, 210009, China

ARTICLE INFO

*Article history:*
Received 4 March 2020
Accepted 24 March 2020
Available online 9 April 2020

*Keywords:*
Pancreatic ductal adenocarcinoma
Kras$^{G12D}$
Loss of heterozygosity
REDD1
Non-canonical glutamine metabolism

ABSTRACT

Pancreatic cancer is associated with high mortality, and pancreatic ductal adenocarcinoma (PDAC) is its most common subtype. The rapid growth of PDAC is dependent on the non-canonical pathway of glutamine (Gln) utilization, and loss of heterozygosity for Kras$^{G12D}$ (Kras$^{G12D}$-LOH) frequently observed in PDAC is associated with an aggressive and invasive phenotype. However, it remains unclear whether Kras$^{G12D}$-LOH contributes to non-canonical Gln metabolism in PDAC. Here, we showed that Kras$^{G12D}$-LOH leads to a substantial increase in non-canonical Gln metabolism in PDAC cells. Importantly, we observed elevated expression of regulated in DNA damage and development 1 (REDD1), which is activated in response to hypoxia and nutrient deprivation, in Kras$^{G12D}$-LOH PDAC, and that REDD1 knockdown efficiently repressed Kras$^{G12D}$-LOH-regulated Gln metabolism and suppressed proliferation, migration, and invasion of Kras$^{G12D}$-LOH PDAC cells. These data provide evidence that REDD1 is a downstream target of Kras$^{G12D}$-LOH and is involved in promoting non-canonical Gln metabolism in PDAC.



## 1. Introduction

Pancreatic ductal adenocarcinoma (PDAC) is the most common among all subtypes of pancreatic cancer, accounting for ~95% of total cases [1]. In recent years, minimal progress has been made in all aspects of therapies in patients with advanced disease [2,3]. The prognosis of PDAC is extremely poor, with only 5% of patients surviving for >5 years after surgery [4]. The late stage at which the majority of patients are diagnosed contributes to their low survival rate [5]. Consequently, unremitting efforts are still required to elucidate the molecular etiology and progress of pancreatic cancer and to define new directions for the development of effective therapeutic strategies for PDAC.

Cumulative evidence demonstrates that KRAS is the predominant mutated isoform in almost all PDAC cases, with its most common oncogenic form encoding Kras$^{G12D}$ [6]. Interestingly, the wild-type allele in PDAC mice harboring Kras$^{G12D}$ is progressively lost, resulting in an increasing incidence of metastasis [7]. Moreover, loss of heterozygosity for Kras$^{G12D}$ (Kras$^{G12D}$-LOH) enhances the proliferative and invasive capacity of PDAC cells [8]; however, the role of this event in PDAC progression has not yet been clarified, and the underlying molecular and cellular mechanisms need to be characterized.

Currently, cancer-related metabolism is considered a promising target for therapeutics and has attracted increasing interest. Many core oncogenic signaling pathways converge to alter tumor cell metabolism to sustain their growth and survival [9]. PDAC is characterized by a hyperactive metabolism, requiring not only increased aerobic glycolysis but also enhanced utilization of the amino acid glutamine (Gln) [10–13]. Unlike most cells that classically metabolize Gln via an α-ketoglutarate (α-KG)-generating mitochondrial pathway, PDAC cells convert glutamate to aspartate and α-KG via the mitochondrial aspartate transaminase (GOT2),

*Abbreviations:* REDD1, regulated in DNA damage and development 1; Gln, glutamine; Kras$^{G12D}$-LOH, loss of heterozygosity for KrasG12D; PDAC, Pancreatic ductal adenocarcinoma; α-KG, α-ketoglutarate; OAA, oxaloacetate; GOT1, GOT2, aspartate transaminase; ROS, reactive oxygen species; mTOR, mammalian target of rapamycin; GLS1, glutaminase; ME1, malic enzyme; MDH1, malate dehydrogenase; sh-RNA, short-hairpin RNA.

* Corresponding author. School of Medicine, Southeast University, Dingjiaqiao 87, Gulou District, Nanjing, 210009, China.
** Corresponding author. Department of Gastroenterology, Southeast University, Dingjiaqiao 87, Gulou District, Nanjing, 210009, China.
*E-mail addresses:* 230159602@seu.edu.cn (M. Hu), hpl@seu.edu.cn (P. Huang).

https://doi.org/10.1016/j.bbrc.2020.03.137

after which Gln-derived aspartate is converted to oxaloacetate (OAA) in the cytoplasm by aspartate transaminase (GOT1) [14]. Additionally, OAA is metabolized to malate and pyruvate, which increase the NADPH: $NADP^+$ ratio and maintain a balance of intracellular reactive oxygen species (ROS) [15] (Fig. 1a). PDAC cells are strongly dependent on this reprogrammed metabolic pathway, which allows them to sustain a rapid proliferation rate [14]. Therefore, it is envisaged that targeting this pathway may represent an effective therapeutic approach for PDAC.

Regulated in DNA damage and development 1 (REDD1) is a stress-response gene expressed in response to hypoxia, nutrient deprivation, and other stress conditions [16]. Moreover, REDD1 has been shown to be a critical upstream regulator of mammalian target of rapamycin (mTOR) [17], a serine/threonine protein kinase relevant to non-canonical anaplerotic Gln metabolism [18]. A previous study demonstrated that upregulated non-canonical Gln metabolism activates mTOR complex 1 in human hepatocellular carcinoma [18]. However, mTORC1 can promote glutamine anaplerosis by upregulating glutamate dehydrogenase (GDH) [19]. Although the role of REDD1 in mTOR regulation has been investigated, its relationship with the non-canonical pathway of Gln utilization has not yet been established.

In the present study, we showed that $Kras^{G12D}$-LOH enhanced non-canonical Gln metabolism accompanied by increased REDD1 expression. Moreover, we found that $Kras^{G12D}$-LOH-induced upregulation of Gln metabolism was inhibited by REDD1 knockdown, which effectively impaired the growth, motility, and invasion of $Kras^{G12D}$-LOH PDAC cells. These findings unveil critical insights into the essential role of REDD1 in Gln metabolism and suggest new potential therapeutic strategies for targeting PDAC cells harboring $Kras^{G12D}$-LOH, which are more aggressive than $Kras^{G12D}$-expressing cells.

## 2. Materials and methods

### 2.1. Cell culture

$Kras^{G12D}$ and $Kras^{G12D}$-LOH cells (hereafter denoted as 399 and 897 cells, respectively) were provided by the Technical University of Munich (Munich, Germany). The cell lines exhibited distinct phenotypes in relation to $Kras^{G12D}$ status. Both cell lines were cultured in DMEM (HyClone, Logan, UT, USA) supplemented with 10% FBS (HyClone) and 100 U/mL penicillin and streptomycin (Beyotime Biotechnology Corporation, Shanghai, China) at 37 °C under normoxic (95% air, 5% $CO_2$) or hypoxic (1% $O_2$, 94% $N_2$, and 5% $CO_2$) conditions.

### 2.2. Gln consumption

Cells were seeded in 6-well plates ($1 \times 10^6$/well) and treated with 2.5 mM Gln under normoxic or hypoxic conditions. Mitomycin was added to inhibit cell proliferation. After a 48-h incubation period, Gln concentration was measured according to the manufacturer's instructions using a Glncolorimetric assay kit (#K556-100; Biovision, Milpitas, CA, USA).

### 2.3. Real-time quantitative polymerase chain reaction (qPCR)

RNAiso Plus reagent (Takara Biotechnology, Dalian, China) was used to isolate total RNA, which was then reverse-transcribed to cDNA using a PrimeScript™ RT master kit (Takara Biotechnology) according to the manufacturer's instructions. Real-time qPCR was conducted and analyzed on the Step One Plus real-time PCR system utilizing a SYBR Premix Ex Taq kit (Takara Biotechnology). The primers used are listed in the Supplementary Material S1.

### 2.4. Western blot

RIPA buffer containing a protease inhibitor (KeyGEN BioTECH, Nanjing, China) was used for cell lysis, and protein concentrations were determined using a BCA protein assay kit (Beyotime Biotechnology Corporation, Shanghai, China). Proteins were separated by 8%–10% SDS-PAGE, followed by transfer to PVDF (Merck Millipore, Billerica, MA, USA). After blocking with 5% non-fat milk at room temperature for 1 h, the membranes were incubated with primary antibodies at 4 °C overnight (the list of primary antibodies is in Supplementary Material S1). The membranes were subsequently incubated with a horseradish peroxidase-conjugated goat anti-rabbit IgG secondary antibody (1:5000; Cat. No. SA00001-2; Proteintech) for 1 h at room temperature. Signals were evaluated by enhanced chemiluminescence (Merck Millipore) and analyzed using ImagePro Plus software (Media Cybernetics, Silver Spring, MD, USA).

### 2.5. Measurement of the NADPH:$NADP^+$ ratio

NADPH:$NADP^+$ ratios were assessed according to the manufacturer's instructions by a NADPH/$NADP^+$ assay kit (A115-1-1; Jiancheng Bioengineering Institute, Nanjing, China). Briefly, cells were divided into two groups (NADPH and $NADP^+$), with the addition of phenazinium methylsulfate (PMS) and glucose-6-phosphate 1-dehydrogenase, respectively, after cell lysis to each group. The concentrations of the two species were then determined by comparison against the relevant standard curves.

### 2.6. Measurement of intracellular ROS levels

Intracellular ROS levels were evaluated according to the manufacturer's instructions using a ROS-detection kit (#E004; Jiancheng Bioengineering Institute). Briefly, cells were initially incubated under normoxic or hypoxic conditions for 48 h and then washed twice with phosphate-buffered saline (PBS), followed by incubation with 30 μM 2,7-dichlorofluorescein diacetate at 37 °C for 1 h. Fluorescence distribution in $2 \times 10^4$ cells was measured using flow cytometry (BD Biosciences, Philadelphia, PA, USA).

### 2.7. Stable transfection of short-hairpin (sh)RNAs

$Kras^{G12D}$ and $Kras^{G12D}$-LOH cells were seeded in 96-well plates ($1 \times 10^4$/well), and transfection experiments were performed upon reaching 40%–60% confluence. Lentiviruses (GenePharma Co, Shanghai, China) were prepared with multiplicity of infection values of 0, 1, 10, 100, and 200 according to the following formula:

MOI = infection titer × lentiviral volume / number of cells to be transfected

where the known lentivirus titer was $1 \times 10^8$ TU/mL. Lentivirus-transfer solution was added according to the different MOI values, and 5 μg/mL of Polybrene was added in each well to improve transfection efficiency. After 72 h–96 h, green fluorescence in cells was observed under a fluorescence microscope (Nikon Eclipse, Tokyo, Japan). Infected cells were cultured for an additional week, followed by transfer to 12-well plates, as needed. Fresh medium containing 2 μg/mL purinomycin was added for an additional culture of 2–3 weeks, after which infected cells were screened for subsequent experiments. REDD1 shRNA sequence (Sense, 5′-3′): GGGATCTTCGACACTTGAAAC and (Antisense, 5′-3′): GTTTCAAGTGTCGAAGATCCC.

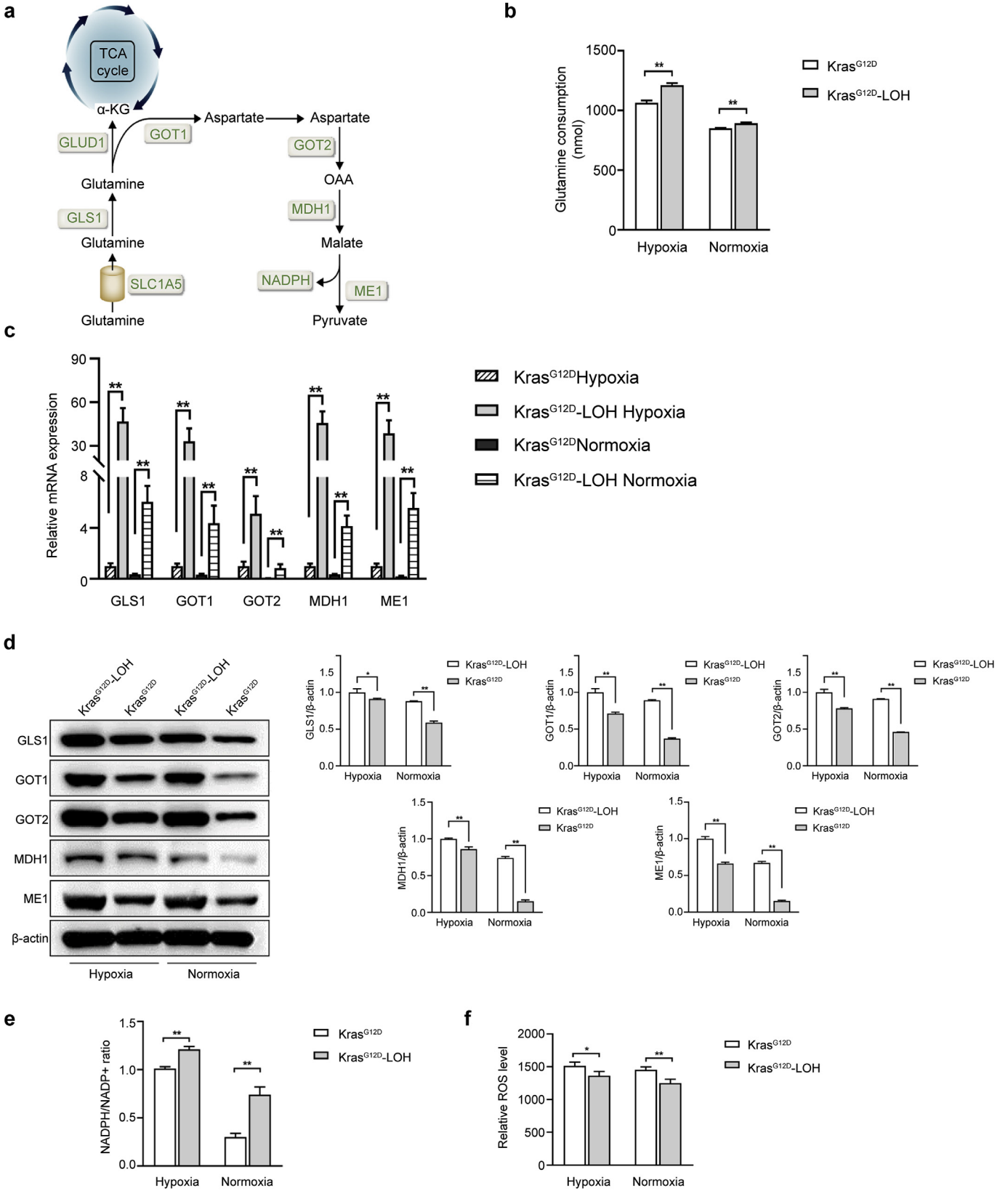


**Fig. 1.** Kras$^{G12D}$-LOH enhances non-canonical Gln metabolism in 399 and 897 PDAC cells exposed for 48 h to normoxic or hypoxic conditions. **(a)** Schematic overview of non-canonical glutamine metabolism in PDAC. **(b)** Gln consumption. **(c)** Assessment of GLS1, GOT2, GOT1, MDH1, and ME1 mRNA levels by qPCR. **(d)** Assessment of GLS1, GOT2, GOT1, MDH1, and ME1 protein levels by western blot. β-actin was used as a loading control. **(e)** NADPH:NADP$^{+}$ ratio and **(f)** intracellular ROS levels. Data represent the mean ± SD from three independent experiments. *$P < 0.05$; **$P < 0.01$. Kras$^{G12D}$-LOH: loss of heterozygosity for Kras$^{G12D}$; Gln: glutamine; GLUD1: glutamate dehydrogenase; α-KG: α-ketoglutarate; OAA: oxaloacetate; GLS1: glutaminase; GOT1, GOT2: aspartate transaminase; MDH1: malate dehydrogenase; ME1: malic enzyme; ROS: reactive oxygen species.

### 2.8. Cell viability assay

Cells were seeded in 96-well plates at $3 \times 10^3$ cells/well (100 μL/well) and incubated for 0 h, 24 h, 48 h, 72 h, and 96 h. The culture medium was then removed, and 10 μL of Cell Counting Kit-8 (CCK-8) solution (Dojindo, Tokyo, Japan) was added to each well. After a 4-h incubation at 37 °C under hypoxic conditions, the optical density at 450 nm ($OD_{450}$) was determined using a spectrophotometric plate reader (Multiskan FC, Thermo, Waltham, MA, USA). The relative percentage of viable cells was calculated as follows: ($OD_{450}$ at detection time/$OD_{450}$at 0 h) × 100.

### 2.9. Colony-formation assay

Cells were seeded in 6-well plates at a density of 300 cells/well and then incubated at 37 °C for 10 days under hypoxic conditions. The colonies were fixed with 4% paraformaldehyde for 30 min and stained with 0.5% crystal violet for 30 min. A cluster containing at least 50 cells was counted as a colony.

### 2.10. Cell-cycle analysis

The cell cycle was assessed using a cell-cycle detection kit (KeyGEN BioTECH). Cells were harvested and washed with cold PBS, followed by the adjustment of cell concentrations to $1 \times 10^6$ cells/mL and fixing in 70% cold ethyl alcohol overnight at 4 °C. The ethyl alcohol was then removed, and RNase A was added, and incubation was carried out for 30 min at 37 °C, followed by staining with 400 μL of propidium iodide (PI) for 30 min at 4 °C. Cell-cycle progression was determined by flow cytometry (Becton Dickinson, Mountain View, CA, USA).

### 2.11. Cell apoptosis assay

Cell apoptosis was measured using an Annexin V-FITC apoptosis detection kit (KeyGEN BioTECH, Nanjing, China). After washing with frozen PBS, the harvested cells were resuspended in 400 μL binding buffer (5 μL Annexin V-FITC and 5 μL PI added) and incubated at room temperature in the dark for 15 min. Data were assessed using flow cytometry (Becton Dickinson, Mountain View, CA, USA).

### 2.12. Wound-healing assay

Cells were seeded in 6-well plates until they attained 80% confluence, after which wounds were created using a 20 μL sterile pipette tip to scratch the surface of the plates. After washing three times with PBS, DMEM containing 2% FBS was added, and the cells were incubated under hypoxic conditions. Cells were photographed at 0 h, 24 h, and 48 h by fluorescence microscopy (Nikon Eclipse, Tokyo, Japan).

### 2.13. Cell-invasion assay

Transwell chambers (8-μm pores; Corning, Corning, NY, USA) were precoated with 50 μL Matrigel (1:3 mixed with FBS-free medium; BD Biosciences) and $5 \times 10^5$ cells in FBS-free medium were plated in the upper chambers. The lower chambers contained 600 μL medium with 10% FBS to trigger the invasion of cells in the upper chambers. After 24-h incubation under hypoxic conditions, a cotton swab was used to remove the cells from the upper membrane. The cells in the bottom chamber were fixed with paraformaldehyde for 30 min and stained with 0.5% crystal violet for 30 min. The number of cells was counted under a microscope (Nikon Eclipse, Tokyo, Japan).

### 2.14. Statistical analysis

All experiments were conducted at least three times independently. Results were expressed as the mean ± standard deviation (SD) and analyzed using one-way analysis of variance (ANOVA) and Student's *t*-tests. Analyses were performed using SPSS software (v.21.0; IBM Corp., Armonk, NY, USA), and a *P* value of <0.05 was considered statistically significant.

## 3. Results

### 3.1. $Kras^{G12D}$-LOH enhanced non-canonical Gln metabolism in PDAC cells under normoxic and hypoxic conditions

The analysis of Gln consumption revealed that under both normoxic and hypoxic conditions, Gln depletion was higher in cells with $Kras^{G12D}$-LOH than in cells without $Kras^{G12D}$-LOH (hereafter referred to as "897 cells" and "399 cells", respectively) ($P < 0.01$) (Fig. 1b). Furthermore, the mRNA and protein levels of enzymes involved in Gln metabolism and determined by qPCR and western blot analyses, respectively, revealed strong upregulation of these enzymes in the 897 cells relative to levels in the 399 cells under both normoxic and hypoxic conditions ($P < 0.01$) (Fig. 1c and d). We consistently observed higher $NADPH:NADP^+$ ratios and lower ROS levels in the 897 cells relative to the 399 cells ($P < 0.01$ and $P < 0.05$, respectively) (Fig. 1e and f). These data indicated that $Kras^{G12D}$-LOH promotes non-canonical Gln metabolism in PDAC cells under normoxic and hypoxic conditions.

### 3.2. $Kras^{G12D}$-LOH increased REDD1 expression in PDAC cells under normoxic and hypoxic conditions

To investigate whether REDD1 has a direct effect on non-canonical Gln metabolism, we examined REDD1 protein levels under normoxic and hypoxic conditions. Notably, REDD1 levels were significantly higher in cells with $Kras^{G12D}$-LOH than in those without $Kras^{G12D}$-LOH under both conditions (Fig. 2a).

### 3.3. REDD1 knockdown suppressed non-canonical Gln metabolism in KrasG12D-LOH PDAC cells

To determine the role of REDD1 in Gln metabolism, REDD1-targeted shRNA or control shRNA was transfected into cells with and without $Kras^{G12D}$-LOH. We confirmed that REDD1 was efficiently knocked down at the protein and mRNA levels by the specific shRNA ($P < 0.01$) (Fig. 2b and c). Additionally, we observed that REDD1 knockdown dramatically reduced Gln consumption in $Kras^{G12D}$-LOH cells under hypoxic conditions ($P < 0.01$) (Fig. 2d). Conversely, a slight increase in Gln consumption was detected in the 399 cells after REDD1 knockdown ($P < 0.05$) (Fig. 2d), with further analyses revealing that REDD1 knockdown repressed GOT1, GOT2, and MDH1 expression in $Kras^{G12D}$-LOH cells at both the mRNA and protein levels ($P < 0.01$) (Fig. 2e and f). Notably, in PDAC cells without $Kras^{G12D}$-LOH, we observed significant increases in GOT1, GOT2, and MDH1 expression following transfection with shREDD1 ($P < 0.05$) (Fig. 2e and f). Moreover, we found a substantially decreased $NADPH:NADP^+$ ratio and enhanced ROS levels in shREDD1 897 cells ($P < 0.05$) (Fig. 2g and h), whereas a significant increase in the $NADPH:NADP^+$ ratio and decrease in ROS levels were observed in shREDD1 399 cells ($P < 0.05$ and $P < 0.01$, respectively) (Fig. 2g and h). These findings suggested that during hypoxia, REDD1 downregulation suppresses non-canonical Gln metabolism in $Kras^{G12D}$-LOH PDAC cells but promotes Gln metabolism in $Kras^{G12D}$ cells.

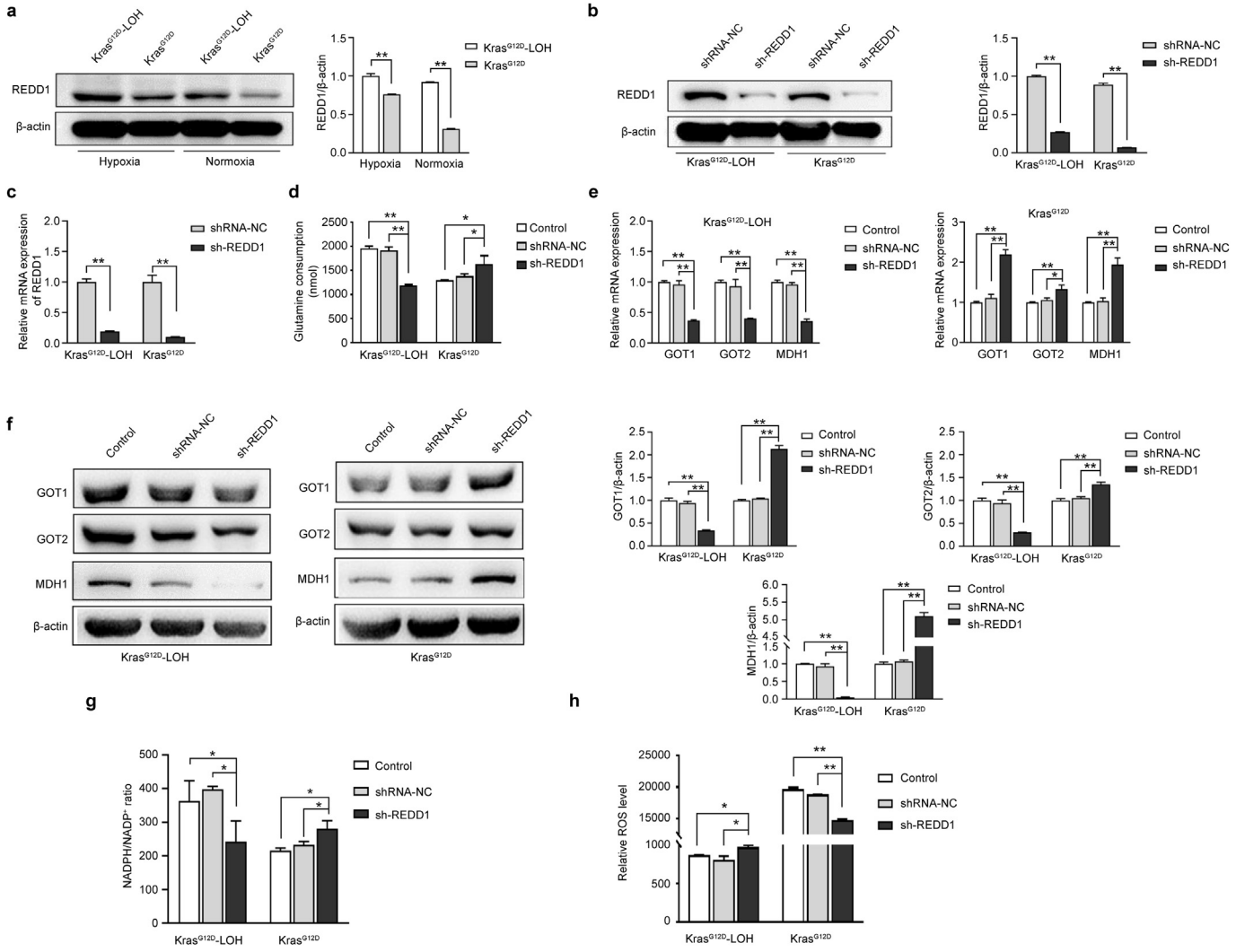


**Fig. 2.** REDD1 knockdown suppresses non-canonical Gln metabolism in Kras$^{G12D}$-LOH PDAC cells. **(a)** 399 and 897 cells were incubated under hypoxic or normoxic conditions, and REDD1 levels were measured by western blot. β-actin was used as a loading control. **(b)** REDD1 levels in 399 and 897 cells transfected with scrambled shRNA and shREDD1 and assessed by western blot. β-actin was used as a loading control. **(c)** REDD1 mRNA levels in 399 and 897 cells transfected with scrambled shRNA and shREDD1 and assessed by qPCR. 399 and 897 cells were transfected with shREDD1 and exposed to hypoxia for 48 h. **(d)** Gln consumption. **(e)** Assessment of GOT1, GOT2, and MDH1 mRNA levels by qPCR. **(f)** Assessment of GOT1, GOT2, and MDH1 protein levels by western blot. β-actin was used as the loading control. **(g)** NADPH:NADP$^+$ ratio and **(h)** intracellular ROS levels. Data represent the mean ± SD from three independent experiments. *$P < 0.05$; **$P < 0.01$. REDD1: regulated in DNA damage and development 1; Kras$^{G12D}$-LOH: loss of heterozygosity for Kras$^{G12D}$; Gln: glutamine; GOT1, GOT2: aspartate transaminase; MDH1: malate dehydrogenase; ROS: reactive oxygen species.

### *3.4. REDD1 knockdown halted the growth of Kras$^{G12D}$-LOH PDAC cells*

Based on the effects of REDD1 knockdown on non-canonical Gln metabolism, we examined whether REDD1 downregulation affects cell growth. CCK-8 analysis revealed a decreased cell-growth rate in shREDD1 Kras$^{G12D}$-LOH cells but an increased rate in shREDD1 Kras$^{G12D}$ cells ($P < 0.01$) (Fig. 3a). Consistently, REDD1 knockdown strongly reduced the number of colonies in Kras$^{G12D}$-LOH cells but increased colonies of cells without Kras$^{G12D}$-LOH ($P < 0.01$) (Fig. 3b). Collectively, these results demonstrated that REDD1 knockdown exerts opposite effects on Kras$^{G12D}$-LOH and Kras$^{G12D}$ cells by impairing and stimulating cell growth, respectively.

### *3.5. REDD1 knockdown blocked cell cycle progression and increased apoptosis of Kras$^{G12D}$-LOH PDAC cells*

Cytometric analyses to establish cell-cycle profiles for shREDD1 897 and 399 cells revealed significantly fewer shREDD1 897 cells in the S phase than in case of the control cells, whereas the number of shREDD1 399 cells entering the S phase was significantly increased relative to the case for the controls ($P < 0.01$) (Fig. 3c). In addition, the apoptosis rate was dramatically increased in 897 cells, compared to the reduction of apoptosis in 399 cells ($P < 0.01$) (Fig. 3d). These results further indicated REDD1 knockdown suppressed the proliferative ability of Kras$^{G12D}$-LOH PDAC cells.

### *3.6. REDD1 knockdown inhibited the migration and invasion of Kras$^{G12D}$-LOH PDAC cells*

The results of a wound-healing assay showed that REDD1 knockdown reduced the motility of 897 cells ($P < 0.01$) (Fig. 4a) but increased the motility of shREDD1 399 cells ($P < 0.01$) (Fig. 4a). Furthermore, REDD1 knockdown significantly decreased the invasion of the 897 cells according to Transwell assays ($P < 0.01$) (Fig. 4b), whereas the invasion of the 399 cells increased markedly

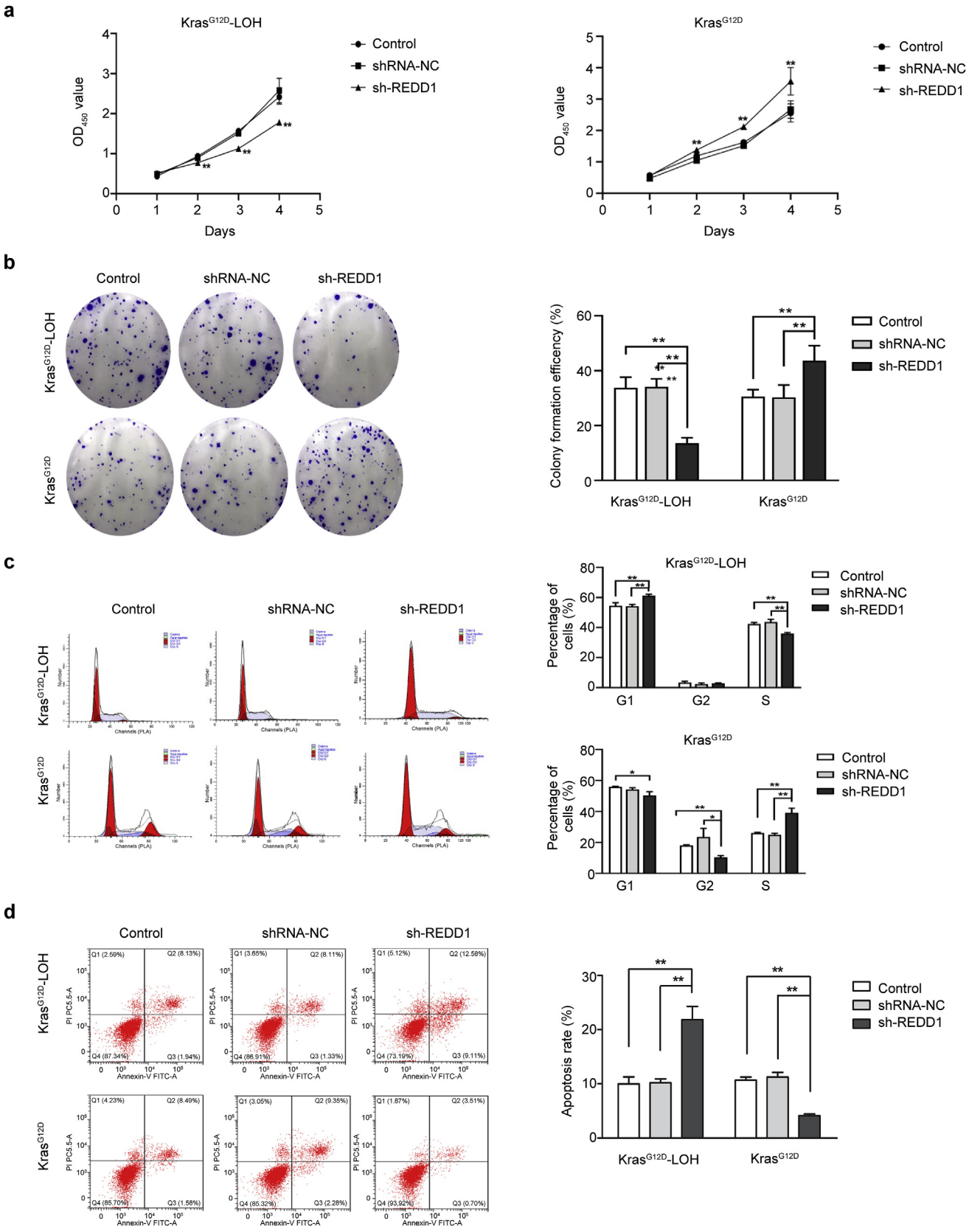


**Fig. 3.** REDD1 knockdown inhibits the progression of Kras$^{G12D}$-LOH PDAC cellsFollowing transfection of the 399 and 897 cells with shREDD1, cells were exposed to hypoxic conditions for 48 h, and various parameters were measured.**(a)** Cell viability measured by CCK-8 assay. **(b)** Assessment of cell proliferation by colony-formation assay. **(c)** Analysis of cell-cycle distribution by flow cytometry. **(d)** Apoptosis rate measured by flow cytometry. Data represent the mean ± SD from three independent experiments. *$P < 0.05$; **$P < 0.01$. REDD1: regulated in DNA damage and development 1; Kras$^{G12D}$-LOH: loss of heterozygosity for Kras$^{G12D}$.

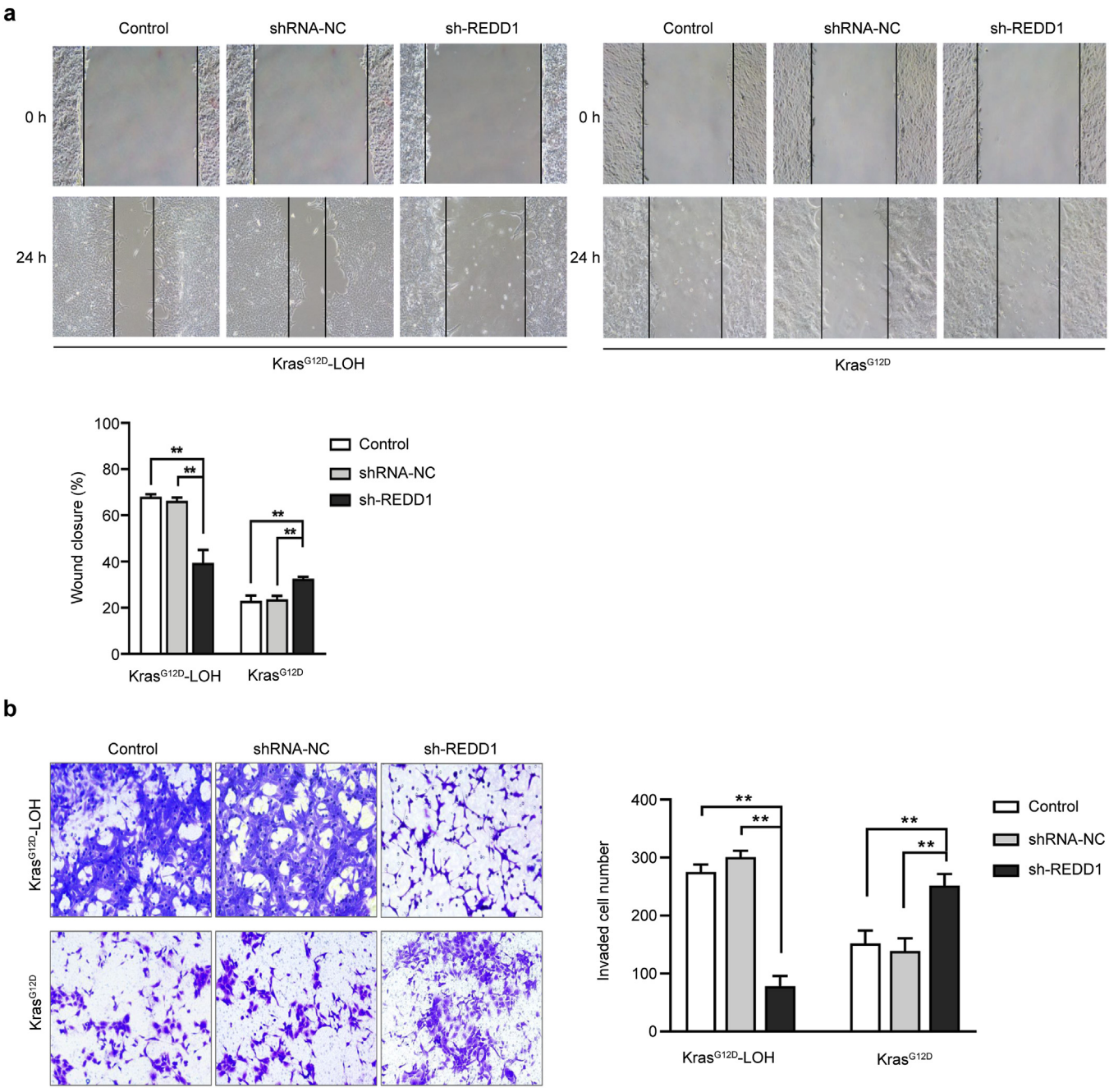


**Fig. 4.** REDD1 knockdown inhibits the migration and invasion of $Kras^{G12D}$-LOH PDAC cells. **(a)** Cell motility of shREDD1-transfected 399 and 897 cells measured by wound-healing assay. **(b)** Invasion of shREDD1-transfected 399 and 897 cells assessed by Transwell assays. Cells were exposed to hypoxic conditions. Data represent the mean ± SD from three independent experiments. $*P < 0.05$; $**P < 0.01$. REDD1: regulated in DNA damage and development 1; $Kras^{G12D}$-LOH: loss of heterozygosity for $Kras^{G12D}$.

after REDD1 knockdown ($P < 0.01$) (Fig. 4b). These results showed that REDD1 knockdown halts the migration and invasion of $Kras^{G12D}$-LOH PDAC cells but promotes these processes in $Kras^{G12D}$ cells.

## 4. Discussion

PDAC is a devastating disease that has developed resistance to traditional cancer therapies through various mechanisms [20]. A recent study reported that PDAC cells maintain uncontrolled growth by reprogramming Gln metabolism, thereby generating interest in anticancer treatments based on the suppression of metabolic processes [16]. Importantly, the alteration of Gln metabolism in PDAC cells is regulated by Kras [16], the mutation of which represents the predominant isoform in PDAC cells, with $Kras^{G12D}$ being the most common oncogenic mutation [6]. Interestingly, loss of heterozygosity for Kras is observed in 37% of primary and 80% of metastatic PDAC cell lines [7]. Notably, $Kras^{G12D}$-LOH promotes the malignant behavior of PDAC cells [8]; however, little is known about the potential correlation between $Kras^{G12D}$-LOH and non-canonical Gln metabolism. In the present study, our data showed that $Kras^{G12D}$-LOH increased the activity of a non-canonical Gln metabolic pathway in PDAC cells and caused REDD1 overexpression. Additionally, we demonstrated that

$Kras^{G12D}$-LOH-mediated promotion of Gln metabolism could be repressed by REDD1 silencing, as REDD1 knockdown effectively attenuated the malignant phenotype of $Kras^{G12D}$-LOH PDAC cells, thereby identifying this factor as a potential therapeutic target.

Metabolic reprogramming is a widely recognized hallmark of cancer. A classic example of this mechanism is the Warburg effect, where tumor cells use glycolysis as a preferential energy source rather than oxidative phosphorylation, even under aerobic conditions [21]. Intriguingly, enhanced glycolytic metabolism is observed in $Kras^{G12D}$-LOH cells relative to that observed in $Kras^{G12D}$ PDAC cells [8], suggesting that $Kras^{G12D}$-LOH provides survival advantages to PDAC cells. Moreover, most cells within solid tumors undergo metabolic alterations to sustain their malignant properties in oxygen- and nutrient-poor environments [22]. For example, hypoxic conditions enable tumor cells to utilize Gln as fuel for ATP production [23]. Additionally, Kras-driven PDAC cells scavenge extracellular proteins to generate Gln and other amino acids to fuel the TCA cycle under nutrient-limited conditions [24]. Moreover, it was recently established that PDAC cells use a non-canonical Gln metabolic pathway to maintain their aggressive growth [16]. In the present study, we showed that $Kras^{G12D}$-LOH strongly upregulated Gln metabolism, indicating that it plays an essential role in the metabolic reprogramming required to meet the bioenergetic demand of malignant PDAC cells.

REDD1 is a negative regulator of mTOR, which, in turn, regulates non-canonical Gln metabolism [25]. Accordingly, we suggest that REDD1 could participate in the regulation of Gln metabolism in $Kras^{G12D}$-LOH PDAC cells. Notably, REDD1 is highly expressed in these cells, and surprisingly, REDD1 suppression effectively prevented the activation of Gln metabolism under hypoxic conditions, leading to inhibited proliferation, migration, and invasion of $Kras^{G12D}$-LOH PDAC cells. Conversely, we found that REDD1 knockdown stimulated Gln metabolism and promoted the malignant behavior of $Kras^{G12D}$ PDAC cells. Moreover, we found that $Kras^{G12D}$-LOH is associated with REDD1 upregulation; however, mTOR is highly activated in $Kras^{G12D}$-LOH cells in contrast to $Kras^{G12D}$ cells [8]. Therefore, the varying effects of REDD1 silencing on $Kras^{G12D}$ and $Kras^{G12D}$-LOH cells may be attributed to $Kras^{G12D}$-LOH-induced stimulation of other pathways to modulate Gln metabolism through REDD1. Unlike in $Kras^{G12D}$-LOH cells, REDD1 strongly relies on the mTOR pathway to regulate Gln metabolism in $Kras^{G12D}$ cells. In agreement with our findings, a previous study showed that $Kras^{G12D}$-LOH promoted glycolysis in PDAC cells in association with both mTOR and REDD1 upregulation [8]. Additional studies are needed to further explore other pathways associated with REDD1-mediated modulation of metabolism in $Kras^{G12D}$-LOH PDAC cells to elucidate its role and mechanism of action.

In summary, we demonstrated that REDD1 plays a central role in mediating non-canonical Gln metabolism, which was enhanced by $Kras^{G12D}$-LOH in PDAC cells under hypoxic conditions. We found that REDD1 knockdown efficiently inhibited activation of non-canonical Gln metabolism, resulting in an impaired malignant phenotype in $Kras^{G12D}$-LOH PDAC cells. The results suggest REDD1 as a potential target for the treatment of highly aggressive $Kras^{G12D}$-LOH PDAC cells.

## Funding

This work was supported by the National Natural Science Foundation of China [grant number 81372152] and the Postgraduate Research and Practice Innovation Program of Jiangsu Province [grant number KYCX17_0183].

## Declaration of competing interest

The authors declare that they have no known competing financial interests or personal relationships that could have appeared to influence the work reported in this paper.

## Acknowledgements

The authors would like to thank Editage (www.editage.com) for English language editing and publication support service.

## Appendix A. Supplementary data

Supplementary data to this article can be found online at https://doi.org/10.1016/j.bbrc.2020.03.137.

## References

[1] D.P. Ryan, T.S. Hong, N. Bardeesy, Pancreatic adenocarcinoma, N. Engl. J. Med. 371 (2014) 1039–1049. https://www.nejm.org/doi/full/10.1056/NEJMra1404198.
[2] M. Hidalgo, Pancreatic cancer, N. Engl. J. Med. 362 (2010) 1605–1617, https://doi.org/10.1056/NEJMra0901557.
[3] M.B. Bagherabad, F. Afzaljavan, S. ShahidSales, et al., Targeted therapies in pancreatic cancer: promises and failures, J. Cell. Biochem. 120 (2019) 2726–2741, https://doi.org/10.1002/jcb.26284.
[4] C.L. Wolfgang, J.M. Herman, D.A. Laheru, et al., Recent progress in pancreatic cancer, CA Cancer J, Clin 63 (2013) 318–348, https://doi.org/10.3322/caac.21190.
[5] T. Kamisawa, L.D. Wood, T. Itoi, et al., Pancreatic cancer, Lancet 388 (2016) 73–85, https://doi.org/10.1016/S0140-6736(16)00141-0.
[6] M.P. di Magliano, C.D. Logsdon, Roles for KRAS in pancreatic tumor development and progression, Gastroenterology 144 (2013) 1220–1229, https://doi.org/10.1053/j.gastro.2013.01.071.
[7] W. Qiu, F. Sahin, C.A. Iacobuzio-Donahue, et al., Disruption of p16 and activation of Kras in pancreas increase ductal adenocarcinoma formation and metastasis *in vivo*, Oncotarget 2 (2011) 862–873, https://doi.org/10.18632/oncotarget.357.
[8] X. Shen, L.G. Chang, M.Y. Hu, et al., $Kras^{G12D}$-LOH promotes malignant biological behavior and energy metabolism of pancreatic ductal adenocarcinoma cells through the mTOR signaling pathway, Neoplasma 65 (2018) 81–88, https://doi.org/10.4149/neo_2018_170224n142.
[9] R. Cairns, I. Harris, T. Mak, Regulation of cancer cell metabolism, Nat. Rev. Canc. (2011) 85–95. https://doi-org.ezproxy.lb.polyu.edu.hk/10.1038/nrc2981.
[10] K. Kawada, K. Toda, Y. Sakai, Targeting metabolic reprogramming in KRAS-driven cancers, Int. J. Clin. Oncol. 22 (2017) 651–659. https://doi-org.ezproxy.lb.polyu.edu.hk/10.1007/s10147-017-1156-4.
[11] C.V. Dang, Links between metabolism and cancer, Genes Dev. 26 (2012) 877–890, https://doi.org/10.1101/gad.189365.112.
[12] I. Regel, B. Kong, S. Raulefs, et al., Energy metabolism and proliferationin pancreatic carcinogenesis, Langenbeck's Arch. Surg. 397 (2012) 507–512. https://doi-org.ezproxy.lb.polyu.edu.hk/10.1007/s00423-012-0933-9.
[13] C.J. Halbrook, C.A. Lyssiotis, Employing metabolism to improvethe diagnosis and treatment of pancreatic cancer, Canc. Cell 31 (2017) 5–19, https://doi.org/10.1016/j.ccell.2016.12.006.
[14] J. Son, C.A. Lyssiotis, H. Ying, et al., Glutamine supports pancreatic cancer growth through a KRAS-regulated metabolic pathway, Nature 496 (2013) 101–105, https://doi.org/10.1038/nature12040.
[15] C.A. Lyssiotis, J. Son, L.C. Cantley, et al., Pancreatic cancers rely on a novel glutamine metabolism pathway to maintain redox balance, Cell Cycle 12 (2013) 1987–1988, https://doi.org/10.4161/cc.25307.
[16] M.D. Dennis, N.K. McGhee, L.S. Jefferson, et al., Regulated in DNA damage and development 1 (REDD1) promotes cell survival during serum deprivation by sustaining repression of signaling through the mechanistic target of rapamycin in complex 1 (mTORC1), Cell. Signal. 25 (2013) 2709–2716, https://doi.org/10.1016/j.cellsig.2013.08.038.
[17] R.A. Saxton, D.M. Sabatini, mTOR signaling in growth, metabolism, and disease, Cell 169 (2017) 361–371, https://doi.org/10.1016/j.cell.2017.02.004.
[18] P. Xu, M.H. Oosterveer, S. Stein, et al., LRH-1-dependent programming of mitochondrial glutamine processing drives liver cancer, Genes Dev. 30 (2016) 1255–1260. http://www.genesdev.org/cgi/doi/10.1101/gad.277483.116.
[19] A. Csibi, S.-M. Fendt, C. Li, et al., The mTORC1 pathway stimulates glutamine metabolism and cell proliferation by repressing SIRT4, Cell 153 (2013) 840–854, https://doi.org/10.1016/j.cell.2013.04.023.
[20] G. Capurso, C. Sette, Drug resistance in pancreatic cancer: new player caught in act, EbioMedicine 40 (2019) 39–40, https://doi.org/10.1016/j.ebiom.2019.02.008.
[21] S.Y. Lunt, M.G. Vander Heiden, Aerobic glycolysis: meeting the metabolic

requirements of cell proliferation, Annu. Rev. Cell Dev. Biol. 27 (2011) 441–464, https://doi.org/10.1146/annurev-cellbio-092910-154237.
[22] R.J. DeBerardinis, N.S. Chandel, Fundamentals of cancer metabolism, Sci. Adv. 2 (2016), e1600200, https://doi.org/10.1126/sciadv.1600200.
[23] J. Fan, J.J. Kamphorst, R. Mathew, et al., Glutamine-driven oxidative phosphorylation is a major ATP source in transformed mammalian cells in both normoxia and hypoxia, Mol. Syst. Biol. 9 (2013) 712, https://doi.org/10.1038/msb.2013.65.
[24] J.J. Kamphorst, M. Nofal, C. Commisso, et al., Human pancreatic cancer tumors are nutrient poor and tumor cells actively scavenge extracellular protein, Canc. Res. 75 (2015) 544–553, https://doi.org/10.1158/0008-5472.CAN-14-2211.
[25] M.P. DeYoung, P. Horak, A. Sofer, et al., Hypoxia regulates TSC1/2-mTOR signaling and tumor suppression through REDD1-mediated 14-3-3 shuttling, Genes Dev. 22 (2008) 239–251. http://www.genesdev.org/cgi/doi/10.1101/gad.1617608.